Optical bistability and collective behavior of atoms trapped in a high-*Q* ring cavity

Th. Elsässer, B. Nagorny, and A. Hemmerich
Institut für Laser-Physik, Universität Hamburg, Luruper Chaussee 149, D-22761 Hamburg, Germany
(Received 23 September 2003; revised manuscript received 17 November 2003; published 12 March 2004)

We study the collective motion of atoms confined in an optical lattice operating inside a high-finesse ring cavity. A simplified theoretical model for the dynamics of the system is developed upon the assumption of adiabaticity of the atomic motion. We show that in a regime where the light shift per photon times the number of atoms exceeds the linewidth of the cavity resonance, the otherwise tiny retroaction of the atoms upon the light field becomes a significant feature of the system. As a result dispersive optical bistability can arise and the lattice positions is determined by the strength of the atom-cavity coupling rather than by the phases of the incoupled light beams. Solving the complete set of classical equations of motion confirms these findings, however, additional nonadiabatic phenomena are predicted, such as, for example, self-induced radial breathing oscillations. We compare these results with experiments involving laser-cooled ^{85}Rb atoms trapped in an optical lattice inside a ring cavity with a finesse of 1.8×10^5. Our observations are in excellent agreement with our theoretical predictions.

DOI: 10.1103/PhysRevA.69.033403 PACS number(s): 32.80.Pj, 42.50.Vk, 42.62.Fi

I. INTRODUCTION

Atoms regularly spaced in an optical lattice are a widely studied model system of quantum optics [1,2] with potential applications in areas ranging from condensed matter physics [3] to quantum information processing [4]. Magneto-optical loading techniques typically provide sparsely populated optical lattices with an average interatomic distance of several microns, where dipole-dipole or spin interactions are negligible. Schemes that provide mutual interactions among the atoms can significantly increase the usefulness of optical lattices. A very successful approach explored by various research groups is to increase the lattice population by loading a Bose-Einstein condensate [5,6]. More recently, the formation of optical lattices inside optical resonators has become a subject of extensive research [7–10], because this can give rise to cavity-mediated long-range interactions even at moderate particle densities. Possible applications range from quantum computing schemes [7] to novel laser cooling methods [11–15] which do not rely on cyclic spontaneous emission and thus apply to a wider class of species without degradation at high densities.

The key to exploiting these new concepts is a profound understanding of the interaction of trapped particles with intracavity light fields with special focus on the external degrees of freedom. For single atoms interacting with only a few photons in cavities with a small mode volume well below 10^{-4} mm^3 studies have been successfully performed within the last few years [16,17]. More recently, large atomic ensembles have been confined in high-finesse cavities with large mode volumes exceeding 1 mm^3. Long trapping times of many seconds could be realized, because disturbing high-frequency intensity noise components of the intracavity light field are significantly suppressed owing to the long photon storage time [8]. Although operation at large detunings from atomic resonance is required in order to prevent undesirable spontaneous emission, for sufficiently high values of the cavity finesse the strong coupling regime can be reached. In this case the interaction strength given by the light shift per photon times the number of trapped particles exceeds the resonance linewidth of the cavity, and thus the otherwise tiny retroaction of the atoms upon the light field becomes a significant feature of the system.

In this paper we experimentally and theoretically explore the motion of atoms trapped in an optical lattice formed inside a high finesse ringcavity with a large mode volume. For strong atom-cavity coupling where the backaction of the atoms upon the lattice potential becomes significant, we find nonlinear dynamics of the intracavity field and a collective character of the atomic motion. In this regime the intracavity field can exhibit dispersive optical bistability, the lattice position is no longer determined by the phases of the incoupled light beams but rather in a self-organization process, and the radial motion can show self-induced breathing oscillations. Absorptive optical bistability due to optical pumping and saturation has been previously observed with resonators operating close to an atomic resonance. Examples include small mode-volume high-finesse resonators with a few cold atoms [19] and low-finesse resonators containing large numbers of cold atoms trapped in a magneto-optic trap [18] or even dense, hot atomic samples confined in a vapor cell [20]. Our lattice operates far from resonance where optical pumping and saturation are negligible and the atoms merely act as a dispersive medium.

The paper is organized as follows. In Sec. II we present a simple physical picture of the atom-cavity coupling in terms of coherent Rayleigh and Bragg scattering. In Sec. III we discuss the complete set of semiclassical equations of motion of the system. These equations are difficult to solve leading us to develop a simplified but surprisingly accurate model of the complex system dynamics based upon the assumption that the atomic sample adiabatically adjusts to the potential position and depth. A steady-state analysis for the phase and amplitude of the intracavity field predicts dispersive bistability. In Sec. IV we summarize the characteristics of our experimental setup. In Sec. V we present experiments in the strong coupling regime which exhibit distinctive nonlinear behavior in excellent agreement with the predictions of the

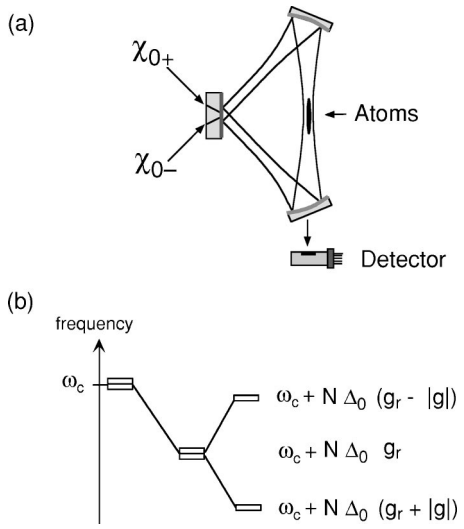

FIG. 1. (a) Sketch of the experimental setup. Adjustable laser powers $\chi_{0\pm}$ are coupled into the two counterpropagating traveling wave modes of a ring resonator. The power transmitted through the cavity can be detected by a photodiode (PD). (b) Mode splitting mechanism (explained in the text).

adiabatic model of Sec. III. In Sec. VI we explore nonadiabatic aspects of the atomic motion. Observations of radial breathing oscillations are discussed and a numerical simulation based on solving the complete set of equations of motion is presented.

II. GENERAL CONSIDERATIONS

The interaction of the atomic sample with the intracavity light field can be understood in terms of coherent Rayleigh and Bragg scattering. Consider the two degenerate, mutually counterpropagating, traveling wave modes of a ring resonator [discriminated by indices $(\pm)$ in the following] with a common resonance frequency ω_c, as depicted in Fig. 1(a). Let us add atoms into the common mode volume with a Bohr frequency $\omega_a \gg \omega_c$ such that their interaction with the intracavity fields has entirely dispersive character. If the atomic sample is homogeneously distributed, it will merely give rise to Rayleigh scattering in the forward directions. This yields equal indices of refraction $n_\pm = 1 - N\, g_r\, \Delta_0/\omega_c$ for both traveling wave modes, where Δ_0 is the light shift per photon (which is negative for the case of normal dispersion considered here), N is the number of atoms, $g_r \equiv (1/N)\Sigma_{\nu=1}^{N} e^{-2(x_\nu^2+y_\nu^2)/w_0^2}$ is the radial bunching parameter, measuring the spatial overlap of the atomic sample with the mode volume, x_ν and y_ν denote the (classical) radial atomic position coordinates, and w_0 is the mode radius. This causes a common frequency shift $N\,\Delta_0\, g_r$ for both modes [Fig. 1(b)].

If the atoms are localized at the sites of a lattice with $\lambda/2$ lattice constant (where λ is the optical wavelength), additional Bragg scattering in the backwards directions can couple the two counterpropagating traveling wave modes. Its efficiency depends on the degree of radial and axial localization measured by the bunching parameter $g \equiv (1/N)\Sigma_{\nu=1}^{N} e^{-i2kz_\nu - 2(x_\nu^2+y_\nu^2)/w_0^2}$, where $k = 2\pi/\lambda$ is the wave number and z_ν denote the (classical) axial atomic position coordinates. This bunching parameter resembles the Debye-Waller factor in the theory of Bragg diffraction from crystalline solids. If there is no statistical correlation between the axial and radial coordinates and the spatial distributions near each lattice site follow a Gaussian, we may write $g = [1 + 4(\sigma_r/w_0)^2]^{-1} \exp(-2k^2\sigma_z^2) \exp(-2ikz_{\mathrm{c.m.}})$, i.e., the complex phase scales with the axial center of mass coordinate $z_{\mathrm{c.m.}} \equiv (1/N)\Sigma_{\nu=1}^{N} z_\nu$ and the modulus is a measure for the axial (σ_z) and radial (σ_r) spread of the atomic sample at each lattice site. Perfect localization corresponds to $|g| = 1$, whereas a homogeneous distribution is described by $|g| = 0$.

Bragg scattering acts to lift the degeneracy of the traveling wave modes giving rise to a pair of resonance frequencies split by $2N\Delta_0|g|$. In the strong coupling regime, i.e., if the interaction parameter $\Delta_0\, N$ exceeds the cavity resonance bandwidth, the corresponding intracavity light fields acquire orthogonal standing wave geometries with either the antinodes or the nodes coinciding with the lattice sites of the atomic grating. In the former case the interaction is maximized and the corresponding frequency shift $\omega_c + N\Delta_0(g_r + |g|)$ exceeds that found for the travelling wave modes in presence of a homogeneous atomic sample. In the latter case the interaction is minimized and a reduced shift $\omega_c + N\Delta_0\,(g_r - |g|)$ applies [Fig. 1(b)].

In our experiments the cavity is initially filled with light in absence of atoms and subsequently atoms are loaded into the antinodes of the intracavity field. The small cavity bandwidth requires that the frequency of the incoupled laser beam needs to by actively controlled in order to maintain some resonance condition. In our implementation we servolock the laser frequency in order to maximize the amplitude of one of the counterpropagating traveling waves [say the $(+)$ mode] with a technique briefly discussed in Sec. IV. For symmetric pumping this yields population of the interaction-maximizing standing wave mode of Fig. 1(b). In this case a stable optical lattice is formed independent of the size of the interaction parameter. The second, not externally pumped mode, blue detuned with respect to the optical lattice, can then be utilized for implementation of a sideband cooling scheme as described in Ref. [14].

For asymmetric pumping of the cavity the situation becomes more complex. Consider the change of the indices of refraction $n_\pm$ experienced by the counterpropagating traveling waves, due to Bragg scattering. In addition to the usual contribution of forward Rayleigh scattering, propagation of the $(\pm)$ wave suffers extra delay from Bragg scattering of the $(\mp)$ wave into the $(\pm)$ wave. This extra contribution should scale with the intensity ratio of the Bragg scattered $(\mp)$ wave and the copropagating $(\pm)$ wave. According to the considerations of Ref. [21] [Eq. (7)], to first scattering order, the modified refractive indices are given by $n_\pm = 1 - N(\Delta_0/\omega_c)(g_r + |g||\alpha_\mp/\alpha_\pm|)$. Note that n_+ and n_- may differ, if the field amplitudes of the traveling waves $\alpha_\pm$ are not equal, e.g., for asymmetric external pumping of the cavity. This gives rise to interesting nonlinear dynamics, if Bragg scattering becomes relevant. A small external pumping asymmetry can yield a relative change of the refractive indi-

ces and a corresponding spatial phase shift of the optical standing wave potential. As the laser frequency is kept actively in resonance with the (+) wave, the (−) wave is tuned slightly out of resonance and the potential well depth decreases. The degree of pumping asymmetry is thus further increased yielding a runaway dynamics which only terminates if the decrease of the degree of localization $|g|$ connected with the decreasing well depth sufficiently reduces the efficiency of Bragg scattering. As we will see in the next section, in a certain parameter range this dynamics allows two steady states to coexist, thus giving rise to bistability phenomena.

III. ADIABATIC MODEL

We restrict ourselves to the case where the cavity modes support coherent fields with large mean photon numbers interacting with large thermal atomic samples at sufficiently high temperatures such that a classical description of the optical intracavity fields and the atomic position and momentum variables is appropriate. Moreover, we assume a large detuning of the pump frequency from the atomic resonance and hence negligible saturation. In this case according to Ref. [22] the following equations describe the time evolution of the complex fields α_+ and α_- for the counterpropagating traveling wave modes scaled to the field per photon:

$$\frac{d}{dt}\begin{pmatrix}\alpha_+\\ \alpha_-\end{pmatrix} = \mathbf{M}\begin{pmatrix}\alpha_+\\ \alpha_-\end{pmatrix} + \gamma_0\begin{pmatrix}\eta_+\\ \eta_-\end{pmatrix},$$

$$\mathbf{M} \equiv \begin{pmatrix} i(\delta_c - N\Delta_0 g_r) - \gamma_c & -iN\Delta_0 g \\ -iN\Delta_0\, g^* & i(\delta_c - N\Delta_0 g_r) - \gamma_c \end{pmatrix}. \quad (1)$$

Here η_+ and η_- are the complex amplitudes of the incoupled light fields, γ_0 is the cavity free spectral range, and δ_c denotes the detuning of the incoupled frequency from the resonance frequency ω_c of the empty cavity. The diagonal elements of the matrix $\mathbf{M}$ comprise the forward (Rayleigh) scattering terms $N\Delta_0 g_r$ which only depend on the degree of radial bunching while the off-diagonal terms which act to couple α_+ and α_- are due to Bragg scattering and thus involve the overall bunching parameter g.

The equations for the momenta $\vec{p}_\nu \equiv (p_{x,\nu}, p_{y,\nu}, p_{z,\nu})$ and the positions $\vec{x}_\nu \equiv (x_\nu, y_\nu, z_\nu)$ read

$$\frac{d}{dt}\vec{p}_\nu = \hbar\Delta_0(\vec{\nabla}|\alpha_+ e^{-ikz} + \alpha_- e^{ikz}|^2 e^{-2[(x^2+y^2)/w_0^2]})\Big|_{\vec{x}=\vec{x}_\nu},$$

$$\frac{d}{dt}\vec{x}_\nu = \frac{1}{m}\vec{p}_\nu. \quad (2)$$

These equations describe the motion of the atoms in the optical potential wells provided by the intracavity fields. In total we are concerned with $6N+2$ coupled first-order nonlinear differential equations for the $3N$ position and momentum variables, respectively and the two complex field amplitudes for the counterpropagating cavity modes.

The incoupled frequency is stabilized such that the complex field amplitude α_+ is maintained at a constant value, i.e., $(d/dt)\alpha_+ \equiv 0$. More precisely, it is the complex phase factor of α_+ which is kept constant, however, as long as $\alpha_\pm$ are sufficiently different from zero this extends to keeping the modulus of α_+ constant as well. Hence, we may combine the two field equations (1) into a single equation for the unlocked mode α_-

$$\frac{d}{dt}\alpha_- = i\frac{\Delta_0 N}{\varepsilon_+} g\alpha_-^2 - \alpha_-\gamma_c - i\Delta_0 N g^* \varepsilon_+ + \varepsilon_-\gamma_c, \quad (3)$$

using the abbreviations $\varepsilon_\pm \equiv (\gamma_0/\gamma_c)\eta_\pm$ for the steady state intra-cavity fields in absence of atoms (scaled to the field per photon). We may choose $\varepsilon_\pm$ to be real without loss of generality, thus fixing the spatial phase of the intracavity standing wave for the case when no atoms are present.

For numerical processing and comparison with experiments it is useful to introduce the quantities $a \equiv \alpha_-/\sqrt{I_0}$ and $\sqrt{\chi_{0\pm}} \equiv \varepsilon_\pm/\sqrt{I_0}$ scaled to the sum $I_0 \equiv |\varepsilon_+|^2 + |\varepsilon_-|^2$ of the steady state photon numbers of the traveling wave modes in absence of atoms. Using the scaled time $\tau \equiv \gamma_c t$ and the scaled light shift per photon $U \equiv \Delta_0/\gamma_c$ we obtain

$$\frac{d}{d\tau}a = i\frac{UN}{\sqrt{\chi_{0+}}}|g|\hat{g}a^2 - a - iUN|g|\hat{g}^*\sqrt{\chi_{0+}} + \sqrt{\chi_{0-}}. \quad (4)$$

In order to incorporate the equations of motion for the atomic ensemble into this equation we seek expressions for the complex phase $\hat{g} = g/|g|$ of the bunching parameter g, which is connected to the atomic center-of-mass coordinate, while the modulus $|g|$ represents the spatial spread of the atomic sample in each potential well. Therefore, let us consider atoms tightly confined in the optical lattice, such that the time scale of the axial motion is much shorter than the photon lifetime $(2\gamma_c)^{-1}$. Recall that $(2\gamma_c)^{-1}$ represents a lower bound for the time scale relevant for changes of the intracavity fields. Consequently, the center-of-mass in each potential well of the optical standing wave should adiabatically follow the potential minimum. We thus assume that the atomic distribution in the lattice can be described by a sum of Gaussians which are centered at the instantaneous antinodes of the lattice. The condition that the center of mass follows the potential well minimum is then formally expressed by the relation $\hat{g}^* = a/|a|$. Recall from Sec. II, that $\hat{g}^*$ for a Gaussian ensemble is equivalent to the complex phase factor $\exp(2ikz_{\text{c.m.}})$ of the center-of-mass $z_{\text{c.m.}}$ and that $a/|a|$ can be written as $\exp(2ikz_{\text{an}})$, where z_{an} modulo $\lambda/2$ denotes the positions of the antinodes. To evaluate $|g|$ we take into account that there is no statistical correlation between the axial and radial coordinates writing $|g| \approx \langle e^{-i2kz}\rangle\langle e^{-2r^2/w_0^2}\rangle$, where the brackets denote a Gaussian average. These expressions are readily calculated to be $\langle e^{-i2kz}\rangle = e^{-2k^2\sigma_z^2}$ and $\langle e^{-2r^2/w_0^2}\rangle = 1/(1+4\sigma_r^2/w_0^2)$. In order to determine the time evolution of σ_r and σ_z we assume that the thermal atomic sample adjusts adiabatically to the potential well depth keeping the Boltzmann factors $\xi_{\text{ax}} \equiv k_B T_{\text{ax}}/\omega_{v,\text{ax}}$ and $\xi_{\text{rad}} \equiv k_B T_{\text{rad}}/\omega_{v,\text{rad}}$ constant, where k_B is the Boltzmann constant and T_{ax} and T_{rad} are the axial and radial temperatures of the sample and $\omega_{v,\text{ax}}$ and $\omega_{v,\text{rad}}$ denote the axial and radial trap frequencies. By harmonically approximating the potential in

axial and radial directions we find $2\sigma_z^2/k^2=\eta_{\mathrm{ax}}\sqrt{a(0)/a(t)}$ and $4\sigma_r^2/w_0^2=\eta_{\mathrm{rad}}[\sqrt{\chi_{0+}}+|a(0)|]/[\sqrt{\chi_{0+}}+|a(t)|]$, with η_{ax} and η_{rad} being the ratio between the thermal energy and the potential depth at $t=0$ for the axial and radial directions, respectively. With these approximations we are in the position to state a single equation for the complex unstabilized electric field amplitude

$$\frac{d}{d\tau}a = i\frac{UN}{\sqrt{\chi_{0+}}}L(a)|a|a - a + \sqrt{\chi_{0-}} - iUN\sqrt{\chi_{0+}}L(a)\frac{a}{|a|},$$

$$L(a) \equiv e^{-\eta_{\mathrm{ax}}\sqrt{|a_0|/|a|}}\frac{1}{1+\eta_{\mathrm{rad}}\dfrac{\sqrt{\chi_{0+}}+|a_0|}{\sqrt{\chi_{0+}}+|a|}}. \tag{5}$$

In this equation all the parameters can be easily obtained by measurements and a numerical integration yields simulations of the intracavity field, that can be compared to experimental data. In Sec. V we will show that despite its simplicity the adiabatic model presented here reproduces our observations very accurately.

We may obtain additional physical insight into the dynamical properties of Eq. (5) by representing the complex field a as $a=|a|e^{i\phi}$ with amplitude $|a|$ and phase ϕ. Multiplying Eq. (5) by $a^*/|a|$ results in separate differential equations for $|a|$ and ϕ:

$$|a|\frac{d}{d\tau}\phi = UNL(a)\left(\frac{|a|^2}{\sqrt{\chi_{0+}}} - \sqrt{\chi_{0+}}\right) - \sqrt{\chi_{0-}}\sin\,\phi, \tag{6}$$

$$\frac{d}{d\tau}|a| = \sqrt{\chi_{0-}}\cos\,\phi - |a|. \tag{7}$$

Equation (7) implicates that the amplitude $|a|$ adjusts exponentially to $\sqrt{\chi_{0-}}\cos\,\phi$ determined by the instantaneous value of ϕ. This happens at the fastest time scale available inside the cavity, the decay time of the intracavity field. Hence, any changes of the intracavity field on slower time scales are governed by the evolution of ϕ. This lets us adiabatically eliminate Eq. (7) by inserting $|a| = \sqrt{\chi_{0-}}\cos\,\phi$ into Eq. (6), which leads to

$$\frac{d}{d\tau}\phi = \frac{UN}{\sqrt{\chi_{0-}\chi_{0+}}}\widetilde{L}(\phi)\left(\chi_{0-}\cos\,\phi - \frac{\chi_{0+}}{\cos\,\phi}\right) - \sqrt{\chi_{0-}}\tan\,\phi,$$

$$\widetilde{L}(\phi) \equiv \frac{\exp\left(-\xi_{\mathrm{ax}}\dfrac{\omega_R}{\omega_V}\sqrt{\dfrac{8}{\sqrt{\chi_{0+}\chi_{0-}}\cos\,\phi}}\right)}{1+\dfrac{8\xi_{\mathrm{rad}}\omega_R}{kw_0\omega_V(\sqrt{\chi_{0+}}+\sqrt{\chi_{0-}}\cos\,\phi)}}. \tag{8}$$

The localization factor $\widetilde{L}(\phi)$ is rescaled in terms of quantities which remain constant during the time evolution of the system, i.e., the axial and radial Boltzmann factors ξ_{ax} and ξ_{rad}, the recoil frequency ω_R, the mode radius w_0, and an effective axial vibrational frequency ω_V which is a measure of the total power directed to the cavity. More precisely, ω_V is the axial vibrational frequency corresponding to the optical potential that would arise for symmetric pumping with no atoms inside the cavity, i.e., if $\alpha_+=\alpha_-=\varepsilon_+=\varepsilon_-$.

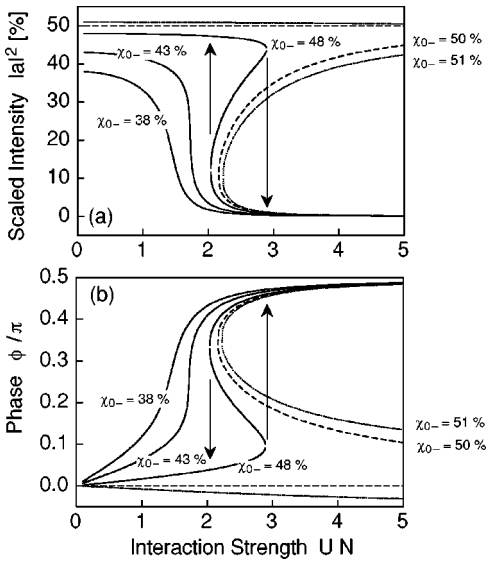

FIG. 2. Steady state solutions of Eqs. (6) and (7) for the intensity (a) and the phase (b) of the unlocked intracavity field for $\chi_{0-}=51,50,48,43$, and 38%. For $\chi_{0-}<43\%$ only one stable solution exists, while for larger values bistability occurs for UN larger than some value around 2. The arrows indicate for the 48% trace, where a jump from one to the other stable solution can occur, if the interaction parameter is tuned.

The dynamical properties of Eq. (5) can be analyzed in terms of its steady state solutions. The steady state values of ϕ are obtained as the zeros of the the right-hand side of Eq. (8) while the corresponding values of $|a|$ follow directly from Eq. (7). It is particularly instructive to plot these steady state values versus the interaction parameter UN, which can be readily tuned experimentally via changing of the particle number N. In Fig. 2 this is shown for different degrees of pumping asymmetry, i.e., $\chi_{0-}=51,50,48,43$, and 38% . In this plot we use our experimental data for $\xi_{\mathrm{ax}},\xi_{\mathrm{rad}},\omega_V,k$, and w_0. For values of $\chi_{0-}<43\%$ only one stable solution exists and the amplitude and phase of the intracavity field a are uniquely defined. The situation changes with increasing χ_{0-}. For higher values, e.g., $\chi_{0-}=48\%$ a bistable regime arises for an interaction parameter of $2\lesssim UN\lesssim 3$. The upper and lower branch with a positive (negative) slope for the phase (amplitude) are stable, whereas the middle branch is unstable. If one increases UN starting from low values on the 48% trace in Fig. 2(a) the system will follow the upper branch until the turning point at $UN\approx 3$ is reached, where the intensity suddenly drops to almost zero. On the other hand, when we reduce the number of particles starting from high values, the intensity abruptly jumps from small to high intensity around $UN\approx 2$. This hysteresis feature is characteristic for bistable systems. If we approach symmetric pumping (i.e., χ_{0-} approaches 50%), the upper bound of the bistability range (the region on the x axis between the jumps) moves further out towards infinity whereas the lower bound only slightly increases above two. For $\chi_{0-}\geqslant 50\%$ the upper bound of the bistability range equals infinity, i.e., the low intensity branch cannot be reached by tuning UN. In this case a stable optical

lattice can be obtained at any value of the interaction parameter.

The two possible steady states feature rather different physical characters. The high intensity branches in the upper left corner of Fig. 2(a) describe the steady state of the weak coupling regime, which basically resembles the familiar steady state of the intracavity field in absence of atoms. Both external light fields [(+) wave and (−) wave] are efficiently coupled into the cavity forming a standing wave (with some traveling wave admixture in case of asymmetric pumping) with antinode positions determined by the phase difference of the incoupled beams. The second steady state described by the low intensity branches in the lower right corner of Fig. 2(a) corresponds to the strong coupling regime. It is characterized by a displacement of the atomic grating of nearly $\pi/4$ with respect to the weak coupling state. In this case the incoupled (−) wave and the Bragg-diffracted portion of the incoupled (+) wave destructively interfere. As a consequence, Bragg scattering of the (+) wave is strongly suppressed and most of the (−) wave is reflected from the cavity. If the pumping asymmetry favors the (+) wave, the Bragg-diffracted portion of the (+) wave exceeds the incoupled (−) wave, i.e., α_- consists mainly of residual Bragg-diffracted (+) wave which explains the $\pi/4$ lattice displacement. The position of the atomic grating is thus determined by the atom-cavity interaction rather than by the phase difference of the incoupled beams. The lattice depth is only a fraction (typically 20% in our experiments) of that found for the weak coupling steady state.

In our analysis we have neglected nonadiabatic aspects of the atomic motion although this is only justified for the axial degrees of freedom which are well confined. Motion along the radial directions occurs on a far slower time scale, and the adiabatic approximation does not hold. A typical nonadiabatic reaction of the radial motion to sudden changes of the potential depth is the excitation of breathing oscillations. Such oscillations would come along with a small oscillatory change of the effective interaction strength. If the system operates deeply inside the bistability regime we may immediately infer from Fig. 2 that small changes of UN with an amplitude well below the extension of the bistability range do not significantly change the intracavity intensity. The most drastic reaction of the intensity to a change of UN occurs, if the system is close to the frontier between stable and bistable operation, as in the 43 % trace of Fig. 2. In this case we in fact observe oscillations of the intensity which are not predicted by our adiabatic model and which are the subject of Sec. V.

IV. EXPERIMENTAL SETUP

Cold ^{85}Rb atoms are prepared with a standard double-MOT (magnetooptical trap) setup as depicted in Fig. 3. In a first vacuum chamber a conventional 3D-MOT collects atoms from a Rb dispenser source. One of the retroreflecting mirrors is provided with a 1.5 mm diameter bore, such that an atomic beam is extracted with a flux of 5×10^8 s^{-1} and a mean velocity of 10 m/s. This beam loads a second magneto-optical trap placed in the main UHV chamber with

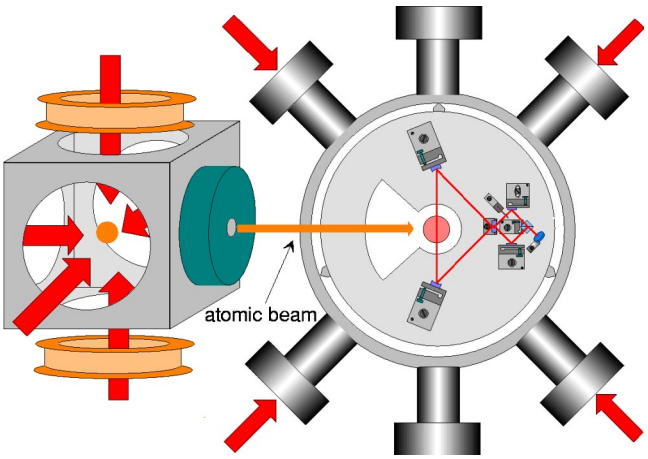

FIG. 3. Sketch of the double-MOT system with the resonator placed in the vacuum chamber.

a pressure below 2×10^{-10} mbar. Here we typically trap 5×10^8 atoms at a temperature of 100μK. The implementation of the MOT coils inside the vacuum permits rapid switching of the magnetic field, however, at the price of contamination emerging via heating of these coils which limits the lifetime of the trap to about 2 s.

The experimental implementation of the resonator is sketched in Fig. 3. In a triangular setup two curved high reflecting mirrors (1.5 ppm transmission) and the flat incoupling mirror (23 ppm transmission) from the high-finesse ring cavity with a round trio path length of 97 mm and a free spectral range of 3.1 GHz. The beam waists w_0 ($1/e^2$ mode radius) in sagittal and vertical directions are 134 and 129 μm, respectively. The beam splitting optics is included in the vacuum to keep the path lengths between the splitter and the incoupling mirror as short as possible. This is favorable because the path length difference influences the spatial phase of the intracavity standing wave.

For the trapping light we use an extended cavity grating stabilized diode laser with around 500 kHz emission bandwidth and variable frequency detuning relative to the $D2$ transition of ^{85}Rb. An acoustooptical modulator serves as a fast switch and an intensity regulator for the lattice. We analyze the reflected and transmitted light with three avalanche photo diodes. In order to stabilize the laser diode emission to the cavity resonance, we use a frequency modulation technique (Pound-Drever-Hall) with a servo bandwidth of several MHz. Similarly as in Ref. [23] the fast branch of the feedback control directly applies the PDH-error signal to the injection current of the diode after passing a loop filter, which compensates for frequency-dependent phase shifts on the diode laser chip. With the laser locked to the resonator we can measure the photon lifetime $2\gamma_c=9.3$ μs corresponding to a finesse of the cavity of $F=1.8\times10^5$, a cavity resonance line width of 17 kHz and a mean scattering loss per mirror of 3 ppm. Because of the small cavity resonance line width, tiny frequency deviations are readily converted into intensity fluctuations, which can lead to exponential heating of the trapped atoms [24]. Steep lattice traps are particular sensitive to this heating mechanism because the heating time scales quadratically with the trap frequency. Fortunately,

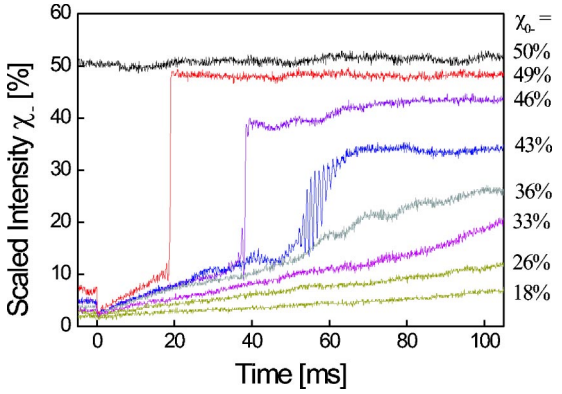

FIG. 4. Scaled intensity χ_- for different values of χ_{0-}. The MOT beams are shut off at $t=0$ ms.

high noise frequencies in the intracavity field are strongly suppressed, because of the long photon storage time, such that our servolock keeps the heating time well below the timescale of a few seconds relevant for our experiments.

V. COMPARISON WITH EXPERIMENTS

The strong coupling regime is accessed if the interaction parameter $\Delta_0 N$ exceeds the decay time of the intracavity field $\gamma_c(UN>1)$. In order to keep the spontaneous scattering time of several ms long enough to avoid significant heating, we operate the lattice at 0.7 nm detuning. This yields a light shift per photom $\Delta_0=0.091\ \mathrm{s}^{-1}$. Hence with a few 10^6 atoms trapped in the lattice we are able to reach values for UN up to 5, well within the strong coupling regime. In the following experiments we have typically applied 5 μW laser power for each traveling wave mode yielding a trap depth of about 800 μK for symmetric pumping and in absence of atoms. The corresponding axial vibrational frequency of 500 kHz is sufficiently larger than the 17 kHz cavity bandwidth, i.e., adiabaticity of the axial motion is a well justified assumption. A typical experiment proceeds in three steps. We superimpose the MOT upon the optical lattice for several seconds, before the MOT light is shut off and the atoms remain trapped in the lattice. Finally, the lattice is extinguished and the atoms are given some time to expand ballistically before a fluorescence image of the sample is taken. From the time of flight the radial temperature of the sample is determined. Without ballistic expansion the fluorescence images give information on the spatial distribution of the trapped atoms. We can continuously tune the ratio of powers in the two running wave modes from the case of symmetric pumping $\chi_{0-}=\chi_{0+}$ to one-sided pumping. We lock the laser frequency to only one of the modes, i.e., χ_+, and keep its phase and amplitude at a constant value. The power leaking out from the unlocked mode through one of the highreflectors is detected and used to determine the scaled intensity χ_-, which corresponds to $|a|^2$ in the theoretical model in Sec. III.

In Fig. 4 we show the time evolution of the scaled intracavity intensity χ_- for different types of pumping. The MOT is terminated at $t=0$ in this figure. For symmetric pumping ($\chi_{0\pm}=50\%$) a stable lattice is formed with equal intensities in each traveling wave mode irrespective of the number of atoms inside the cavity. For values of χ_{0-} below 50% the situation changes drastically. For an asymmetry of only 1% in favor to the locked mode the intracavity intensity χ_- drops to about 10% during the MOT phase and to almost zero after shutting off the MOT beams. Subsequently, a slow increase is observed before at about 20 ms the intensity suddenly jumps back to nearly the value χ_{0-} (the value expected in absence of atoms) with a rise time below a few hundred microseconds. If the power of the unlocked mode is further reduced, the time duration before the jump occurs increases as well as the rise time until the jump completely vanishes for values $\chi_{0-}<40\%$. At a value of ($\chi_{0-}=43\%$), where the jump begins to level off, strong oscillations of roughly 1 kHz are observed corresponding to twice the radial vibrational frequency. The traces for asymmetric pumping in Fig. 4 are observed for χ_{0-} adjusted to 49, 46, 43, 36, 33, 26, and 18%, respectively. The corresponding values of the initial interaction parameter $UN(t=0)\approx 4.48$, 4.25, 4.01, 3.54, 3.30, 2.95, 2.48 are carefully determined by measuring the initial particle number $N(t=0)$ via fluorescence detection. The observed decrease of $N(t=0)$ with decreasing χ_{0-} arises because the capture efficiency decreases with the lattice well depth.

In our experiments the value of the interaction parameter necessarily decreases with time due to trap loss. The corresponding decrease of UN in connection with the bistability plot of Fig. 2(a) explains the observations of Fig. 4. As time proceeds in Fig. 4 we move from right to left in Fig. 2(a) starting on one of the low intensity branches in the lower right corner. Hence, depending on the value of χ_{0-} we encounter a sudden or soft increase of intensity, depending on whether we travel on a curve with bistable or stable character. We also adjusted values of χ_{0-} above 50%. In this case χ_- initially drops to a value close to 50 % independent of the value of χ_{0-} and gradually recovers to χ_{0-}. This behavior is understood by similar arguments based on Fig. 2.

We have simulated the time evolution observed in Fig. 4 by means of Eq. (5). The values of $|a_0|$ are taken directly from the observations of Fig. 4(a) for $t=0$. The values of $\eta_{\mathrm{ax}}=0.5$ and $\eta_{\mathrm{rad}}=0.3$ are determined by temperature measurements with an uncertainty of about 0.1. The difference in the radial and axial directions originates from different trap depths for both directions, since the contrast of the interference pattern in axial direction depends on the degree of pumping asymmetry. The decrease of $N(t)$ with time is derived from trap lifetime measurements analyzed by means of a standard trap decay model including a two-body loss term. The theoretical simulations shown in Fig. 5 reproduce our experimental traces very nicely. Not only the general behavior of the jump feature, but also the time of the jump to occur, is accurately matched. For the initial interaction parameter UN we used the values 2.38, 2.23, 2.15, 1.75 for χ_{0-} being 49, 46, 43, and 36%, which fall within a few percent of those determined for the corresponding experimental traces, however reduced by a common scaling factor 1.89. The need for this factor is not surprising, because in our atom number measurements up to a factor two uncertainty should be expected for the absolute values, while relative values are on the few percent level.

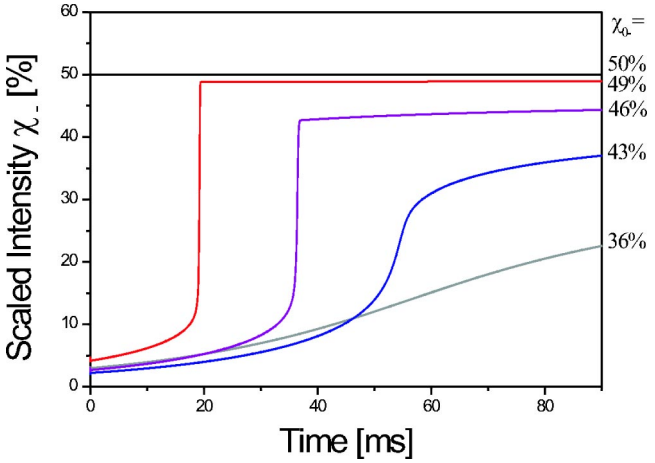

FIG. 5. Theoretical simulations of the experimental observations of Fig. 4.

In the strong coupling regime our system shows an anomalous response to a change of the total intensity coupled to the cavity while keeping the same pumping asymmetry. This is shown in Fig. 6(a) for $\chi_{0-}=45\%$. In this plot we have reduced I_0 by a factor 2 at $t=0$ ms and doubled it again at $t=2$ ms. As a first immediate reaction to the reduction χ_- rapidly drops on a time scale given by the cavity decay time γ_c^{-1}, as might be expected. However, this is counteracted by an approach of an increased steady state value on a slower time scale. When the old power level is reestablished, after a transient increase, χ_- drops back to nearly its original value. A numerical simulation based on our adiabatic model of Sec. V reproduces the experimental findings surprisingly well except for an unexplained additional ripple at about 3 kHz, which amounts to about six times the radial vibrational frequency. The calculations also show that during the drop of I_0

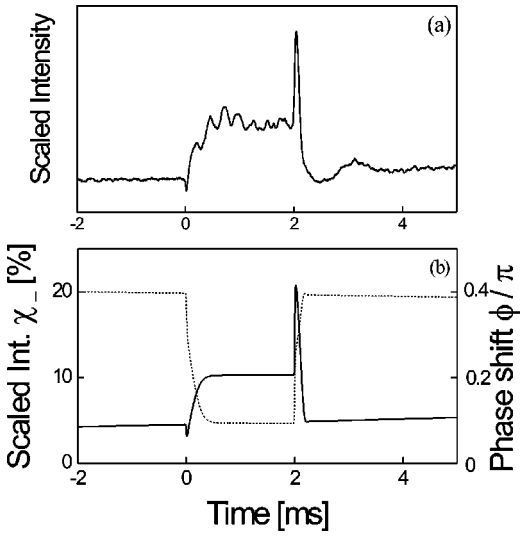

FIG. 6. (a) Observed intensity of the unlocked mode plotted versus time. During the time interval $0\ \text{ms}<t<2\ \text{ms}$ the total power coupled to the cavity is reduced by factor of 2. (b) A numerical simulation based on the adiabatic model. The intensity χ_- (solid line) and the corresponding phase ϕ (dotted line) are shown.

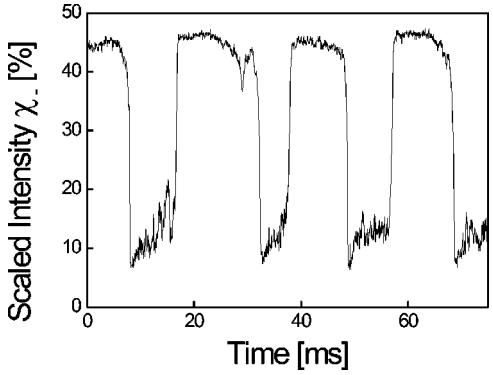

FIG. 7. Bistable switching of χ_- during MOT loading for $\chi_{0-}=49\%$.

the phase shift of the unlocked mode with respect to the locked mode is reduced. Therefore the effective wavelength of the unlocked mode is shifted closer to resonance and the intensity increases.

The bistable character of the atom-cavity system can also be observed at work during MOT loading, yielding plots as that shown in Fig. 7, where χ_- switches between two steady state solutions ($\chi_{0-}=49\%$). Starting at $t=0$ at the high intensity level and hence with a deep lattice with comparably low atom number N, the MOT tends to increase N until the interaction parameter exceeds the critical value and a jump occurs. Now the intensity is low and hence the lattice depth, while the temperature remains the same. This yields a decrease of the loading rate and thus a reduction of N until the system jumps back to the previous state.

In order to control the performance of the locking the light reflected from the cavity originating from the locked traveling wave mode is monitored together with the light of the unlocked mode transmitted through one of the high reflectors. This allows us to verify that despite of the rapid changes in time observed for χ_- and ϕ, the intracavity intensity of the counterpropagating locked mode remains well behaved. This is illustrated in Fig. 8 for $\chi_{0-}=45\%$. While in the lower trace rapid time evolution is observed the upper trace remains nicely constant. The residual structure seen in the

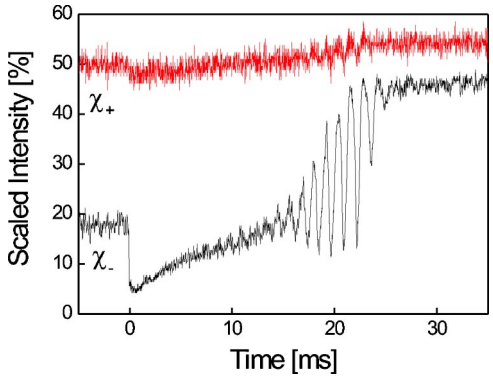

FIG. 8. The intracavity intensities χ_- and χ_+ of the unlocked mode (lower trace, recorded in transmission) and the locked mode (upper trace, obtained from the reflected light) are plotted versus time for $\chi_{0-}=45\%$.

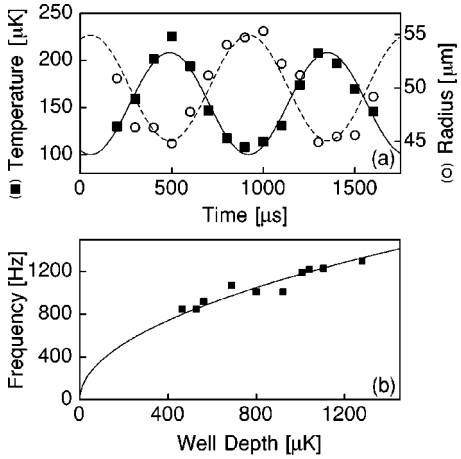

FIG. 9. (a) Oscillation of the atomic position spread (circles) and momentum spread (rectangles). The solid and dashed lines are trigonometric fits with π phase delay. (b) Oscillation frequency plotted versus the well depth. The solid line shows the expected square-root dependence.

upper trace is explained by imperfect separation of the contributions from the two modes due to limited quality of the polarization optics used.

VI. NONADIABATIC MOTION

The adiabatic model excellently explains the experimental findings regarding the intracavity intensity except for the pronounced oscillation feature observed in the $\chi_{0-}=43\%$ trace of Fig. 4. As has been discussed at the end of Sec. III the assumption of adiabaticity is not well justified for the radial degrees of the atomic motion. We came to the conclusion that for fast changes of the lattice well depth breathing oscillations should be excited which would produce corresponding oscillations in the intracavity intensity, if the system is operated near the frontier between the stable and the bistable regime, i.e., in the 43% trace of Fig. 2. In fact this oscillation is observed in Fig. 4. An expanded version is shown in Fig. 10(a).

As an experimental test of our interpretation in terms of radial breathing oscillations we have measured the momentum and position spread of the atomic ensemble in the radial direction during the observed intensity oscillations, finding the behavior shown in Fig. 9(a). The black rectangles show the radial momentum spread of the atomic sample determined by time-of-flight measurements, while the open circles show the radial spread directly observed via *in situ* images of the atoms in the lattice. The solid and dashed lines are trigonometric fits with π phase delay, which confirm the expected anticyclic behavior. In Fig. 9(b) we plot the frequency of the observed intensity oscillations versus the potential well depth which is consistent with the expected square-root dependence.

In order to include nonadiabatic aspects in our theoretical description we use the full set of $6N+2$ equations of motion of Eq. (4) and Eq. (2) (i.e., $6N$ equations for the atomic positions and momenta and two equations for the amplitude and the phase of the unlocked intracavity mode). Since these equations are coupled and nonlinear, the simulation of all 10^6 atoms is beyond our computational capacities. Therefore, in our calculations we reduce the number of atoms to one hundred and work with an increased light shift per photon, such that the interaction parameter acquires values which compare to the experiments. The artificially increased light shift per photon comes along with a correspondingly increased light shift acting on each atom. Hence, in order to maintain the potential well depth at the level used in the experiments, we work with correspondingly decreased incoupled intensities.

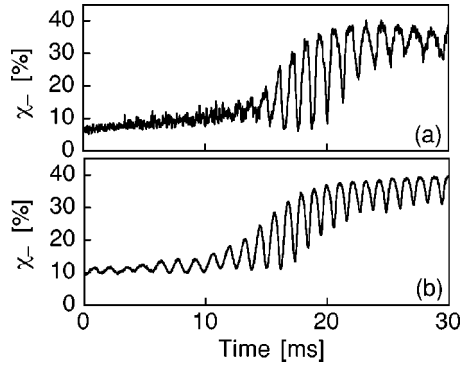

FIG. 10. (a) Experimental observation of radial breathing oscillations. (b) Simulation of the oscillations of (a) by means of solving the complete set of equations of motion for hundred atoms with an upscaled interaction parameter.

The full model for one hundred atoms very accurately reproduces our calculations based on the adiabatic model shown in Fig. 5 except for the fact that in the vicinity of $\chi_{0-}\approx 43\%$ additional oscillations arise. This confirms once again that the assumption of adiabaticity of Sec. V is well justified for the axial degrees of freedom. We can quantitatively reproduce the frequency of the breathing oscillation as is shown in Fig. 10(b). The experimental data are taken for $UN\approx 3.5$ and an axial vibrational frequency of 500 kHz, whereas for the theoretical curve $UN=2.0$ and 550 kHz was used. Applying the scaling factor 1.89 compensating for our systematic overestimation of the atom number similarly as in Sec. V the measured interaction parameter coincides with the theoretical value within 10 %. The discrepancy in the vibrational frequencies lies within our observation uncertainty of around 10 %.

VII. CONCLUSIONS

We conclude that optical lattices formed inside high finesse cavities open up an interesting new regime characterized by collective interactions which significantly contribute to the atomic dynamics. This regime can be experimentally realized even far from an atomic resonance such that the atom-light interaction is entirely dispersive. In the ring cavity studied here, specific parameter ranges are identified which allow us to operate a stable lattice independent of the number of trapped atoms. Other regimes are found where dispersive optical bistability accompanied by self-induced breathing oscillations occur. The spatial phase of the lattice is not pinned

by the phases of the incoupled laser beams, but rather determined by the strength of the atom-cavity interaction. Bistable behavior arises for asymmetric pumping and can be understood in terms of an adiabatic approximation for the atomic motion, whereas the general equations of motion must be considered to model the observed breathing oscillations. In this article we have only discussed selected aspects of the system dynamics. Other interesting phenomena could be studied, as for example collective atomic recoil lasing [25], which has been recently observed for unidirectional pumping of the ring cavity [26]. The strong coupling regime might also be utilized for implementing novel laser cooling schemes, which rely on cavity-tailored coherent scattering, for example, as described in Ref. [14]. Such schemes are highly desirable since they promise to extend laser cooling to new species and to operate in a density regime not yet accessible.

ACKNOWLEDGMENT

This work has been supported by Deutsche Forschungsgemeinschaft (DFG) under Contract No. *He*2334/3−2.

[1] G. Grynberg and C. Robilliard, Phys. Rep. **355**, 335 (2001).
[2] R. Grimm, M. Weidemüller, and Y. B. Ovchinnikov, Adv. At., Mol., Opt. Phys. **42**, 95 (2000).
[3] D. Jaksch, C. Bruder, J. I. Cirac, C. W. Gardiner, and P. Zoller, Phys. Rev. Lett. **81**, 3108 (1998).
[4] T. Calarco, H.-J. Briegel, D. Jaksch, J. I. Cirac, and P. Zoller, J. Mod. Opt. **47**, 2137 (2000).
[5] B. Anderson and M. Kasevich, Science **281**, 1686 (1998).
[6] M. Greiner *et al.*, Nature (London) **415**, 39 (2002).
[7] A. Hemmerich, Phys. Rev. A **60**, 943 (1999).
[8] B. Nagorny *et al.*, Phys. Rev. A **67**, 031401(R) (2003).
[9] B. Nagorny, Th. Elsässer, and A. Hemmerich, Phys. Rev. Lett. **91**, 153003 (2003).
[10] D. Kruse *et al.*, Phys. Rev. A **67**, 051802(R) (2003).
[11] A. C. Doherty, A. S. Parkins, S. M. Tan, and D. F. Walls, Phys. Rev. A **56**, 833 (1997).
[12] P. Horak *et al.*, Phys. Rev. Lett. **79**, 4974 (1997).
[13] G. Hechenblaikner, M. Gangl, P. Horak, and H. Ritsch, Phys. Rev. A **58**, 3030 (1998).
[14] Th. Elsässer, B. Nagorny, and A. Hemmerich, Phys. Rev. A **67**, 051401(R) (2003).
[15] H. W. Chan, A. T. Black, and V. Vuletic, Phys. Rev. Lett. **90**, 063003 (2003).
[16] P. W. H. Pinkse, T. Fischer, P. Maunz, and G. Rempe, Nature (London) **404**, 365 (2000).
[17] C. Hood *et al.*, Science **287**, 1457 (2000).
[18] A. Lambrecht, E. Giacobino, and J. M. Courty, Opt. Commun. **115**, 199 (1995).
[19] J. A. Sauer *et al.*, quant-ph/0309052 (unpublished).
[20] A. Joshi and M. Xiao, Phys. Rev. Lett. **91**, 143904 (2003).
[21] M. Weidemüller, A. Görlitz, Th. W. Hänsch, and A. Hemmerich, Phys. Rev. A **58**, 4647 (1998).
[22] M. Gangl and H. Ritsch, Phys. Rev. A **61**, 043405 (2000).
[23] A. Schoof, J. Grünert, S. Ritter, and A. Hemmerich, Opt. Lett. **26**, 1562 (2001).
[24] T. A. Savard, K. M. O'Hara, and J. E. Thomas, Phys. Rev. A **56**, R1095 (1997).
[25] R. Bonifacio, L. De Salvo, L. M. Narducci, and E. J. D'Angelo, Phys. Rev. A **50**, 1716 (1994).
[26] D. Kruse, C. von Cube, C. Zimmermann, and Ph. Courteille, Phys. Rev. Lett. **91**, 183601 (2003).